StarDICE: a photometric calibration experiment to anchor standard stars on the NIST flux scale at the milli-magnitude level

T Souverin, J Neveu, M Betoule, S Bongard, P.E Blanc, J. Cohen Tanugi, S Dagoret-Campagne, F Feinstein, M Ferrari, F Hazenberg, et al.

StarDICE: a photometric calibration experiment to anchor standard stars on the NIST flux scale at the milli-magnitude level

T. Souverin[1], J. Neveu[1, 3], M. Betoule[1], S. Bongard[1], P. E. Blanc[5], J. Cohen Tanugi[2, 6], S. Dagoret-Campagne[3], F. Feinstein[4], M. Ferrari[5], F. Hazenberg[1], C. Juramy[1], L. Le Guillou[1], A. Le Van Suu[5], M. Moniez[3], E. Nuss[2], B. Plez[2], N. Regnault[1], E. Sepulveda[1], and K. Sommer[2]

[1]Sorbonne Université, CNRS, Université de Paris, LPNHE, 75252 Paris Cedex 05, France
[2]LUPM, Université Montpellier & CNRS, F-34095 Montpellier, France
[3]Université Paris-Saclay, CNRS, IJCLab, 91405, Orsay, France
[4]Aix Marseille Univ, CNRS/IN2P3, CPPM, Marseille Cedex 09, France
[5]Aix Marseille Univ, CNRS/IN2P3, Observatoire de Haute-Provence, 04870 Saint Michel L'Observatoire, France
[6]LPC, IN2P3/CNRS, Université Clermont Auvergne, F-63000 Clermont-Ferrand, France

ABSTRACT

The number of type Ia supernova observations will see significant growth within the next decade, especially thanks to the Legacy Survey of Space and Time (LSST) undertaken by the Vera Rubin Observatory in Chile. With this improvement, statistical uncertainties will decrease and flux calibration will be one of the dominant sources of systematic uncertainties for the characterization of dark energy. To address this issue, the StarDICE experiment proposes to recalibrate the spectra of CALSPEC standards stars at the millimagnitude level, securing calibration reference for any SNe Ia survey. The StarDICE experiment is currently operating at l'Observatoire de Haute-Provence and has been taking data since the beginning of 2023. To reach a sub-percent precision, the instrument throughput will be monitored with an LED-based artificial star source, calibrated on NIST photodiodes. I present here the first results of the StarDICE photometric analysis, and the predicted performance to recalibrate the CALSPEC standard stars.

Keywords: Cosmology, SNe Ia, Photometric calibration, Standard stars, Metrology chain

1. INTRODUCTION

Cosmological studies relying on type Ia supernovæ (SNe Ia) will soon benefit from a large number of observations thanks to large surveys such as ZTF (Zwicky Transient Facility), DES (Dark Energy Survey), HSC (Hyper Suprime-Came), or LSST (Large Synoptic Survey Telescope). As the statistical uncertainties decrease, the survey instrument will need an increasingly precise photometric calibration. The light curve produced by any SN Ia, i.e. its luminosity with respect to time, is predictable and rather consistent and can be standardized at the 15 % level. Consequently, we say that SNe Ia are "standard candles", which we can use to characterize the dark energy equation of state. By measuring the luminosity distances of SNe Ia across various redshifts, it is possible to draw a Hubble diagram, a tool used to probe the Universe's expansion dynamics.

These luminosity distances are determined by measuring the maximum amplitude of the SNe Ia light curves, which are observed through different telescope bands depending on their redshift. Thus, chromatic errors in the relative flux calibration between these bands can lead to systematic errors in the Hubble diagram, consequently affecting the constraints on dark energy parameters. This issue becomes more pronounced when multiple surveys are combined in a single analysis, increasing the number of bands involved. A major challenge lies in the

Further author information:
T. Souverin: E-mail: thierry.souverin@lpnhe.in2p3.fr,
J. Neveu: E-mail: jeremy.neveu@lpnhe.in2p3.fr

photometric calibration of the survey instruments, especially in achieving consistent color calibration across all the bands. This issue is usually addressed by observing standard stars with calibrated spectra. Each survey instrument can observe these standards to achieve precise chromatic calibration of their bandpasses, ultimately aligning all surveys on a unified photometric scale.

The current state of the art consists of a network of 121 stars spectra provided by the CALSPEC calibration from Bohlin et al. 2020[1], which can be observed by any survey to calibrate their instrument. This calibration relies on numerical models of stellar atmospheres of 3 primary standards. These primary standards are DA white dwarfs (DA WDs), a category of star mainly composed of hydrogen, with at most traces of other elements. DA WDs have been chosen because modeling their atmospheres relies almost only on one chemical neutral element, significantly simplifying the calculations. The three selected WDs are GD153, GD71, and G191B2B, and their atmosphere "Spectral Energy Densities" (SEDs) have been calculated in the assumption of a non-local thermodynamic equilibrium (NLTE).[2] The comparison between the model and observed fluxes of 35 DA WDs has been studied in Axelrod et al. 2023,[3] where they manage to reach a consistency below 0.004 mag from 2700 to 7750 Å, and extended the models to fainter stars.

However, the current DA WD calibration approach is based on one important assumption: the DA WD atmosphere models are fully representative of reality. In the last release from Bohlin et al. 2020[1] several aspects can be discussed. Different models are used to calibrate G191B2B compared to GD153 and GD71, with variations such as the inclusion or exclusion of a mask for metal absorption lines. Additionally, the absence of convection considerations in the DA WD atmospheres could introduce errors. The models have also evolved between different releases, leading to varying results for the calibrated spectra. These relative differences reveal chromatic discrepancies of up to ∼2 % between different CALSPEC releases, as it is shown in the Figure 8 of Bohlin et al. 2020.[1] Despite the theoretical calculations improvements, the level at which models are representative of reality remains a blind spot that should not be ignored.

The StarDICE experiment aims to address this issue by establishing a metrology chain from laboratory flux references toward the measurement of CALSPEC standards. This endeavor necessitates multiple steps of laboratory calibration transfers, ultimately providing a photometric calibration of an artificial light source composed of 16 LEDs covering the visible wavelength range. This artificial light source is then set up far enough to appear as a point-like source to the observer, providing an artificial star of controlled flux. By observing alternatively the StarDICE artificial star and the CALSPEC stars, it is possible to achieve a recalibration of the CALSPEC standard stars with the StarDICE telescope.

When observing astrophysical sources with the StarDICE telescope, two major physical components must be considered: the bandpass filter transmission and the atmospheric transmission. The former will be monitored throughout the survey using the StarDICE artificial star, calibrated in the laboratory. Additionally, a redundant calibration path is provided by the Collimated Beam Projector (CBP), as detailed in Souverin et al. 2022.[4] To account for atmospheric transmission, observations of the same target at different elevations are conducted. Another study on the atmosphere transmission is pursued with a diffraction grating set in the filterwheel, allowing for slitless spectrophotometry with the Spectractor software*. By performing an airmass regression, and comparing the observations with synthetic photometry, we can estimate the out-of-the-atmosphere magnitude of the target In this paper we present our data and methodology and discuss the predicted performances of the StarDICE experiment in recalibrating the CALSPEC standard stars

Section 2 provides an overview of the current status of the StarDICE experiment. In Section 3, we describe the dataset obtained with the StarDICE telescope, and the method used to produce the synthetic photometry, both used to achieve photometric analysis. Section 4 presents the photometric analysis and the results of the prediction performance of the StarDICE telescope after a two-year survey. Finally, Section 5 discusses the findings and future perspectives.

*https://github.com/LSSTDESC/Spectractor

2. OVERVIEW OF THE StarDICE EXPERIMENT

2.1 Concept of the experiment

The metrology chain developed by the StarDICE experiment is represented in Figure 1, which illustrates the complete calibration transfer from the optical watt defined by the NIST to SNe Ia observations. Here are the detailed stages of the calibration transfer, following the notation from Figure 1: (1) is operated by the NIST described in Houston et al. 2008,[5] and results in a silicon photodiode calibrated against the POWR[†] facility; (2) is achieved with the StarDICE sensor calibration bench, an automated spectrophotometric bench built to perform the calibration transfer between two sensors from Betoule et al. 2023[6]; (3) consists of the calibration of the StarDICE artificial star with the previously calibrated StarDICE camera; (4) is the recalibration of the CALSPEC standard stars with the calibrated telescope, achieving the photometric analysis detailed in Section 4; (5) is performed by the survey to calibrate its instrument by observing the standard stars, yielding more accurate measurements for SNe Ia cosmology.

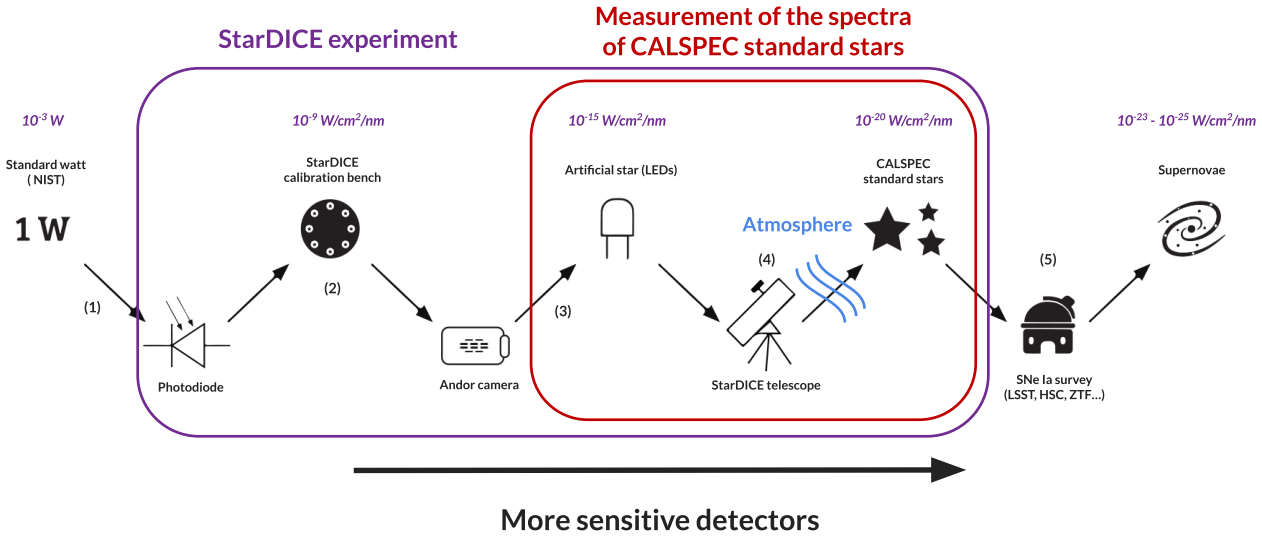

Figure 1. Calibration transfer of the StarDICE experiment, from the standard watt defined by the NIST to the measurement of a type Ia supernovæ. The top row corresponds to the sources, while the bottom shows the detectors. The purple box represents every step undertaken by the StarDICE experiment, while the red box shows the calibration of the standard stars. Every step of this transfer aims to calibrate more sensitive detectors and goes through approximately 20 orders of magnitude of luminosity.

2.2 Setup description

The StarDICE photometric instrument is composed of a Newton telescope with a 16 inches (~ 40 cm) diameter primary mirror and a 1.6 m focal length ($f/D = 4$), and an Andor Ikon-M DU934P-BEX2-DD camera at its focal plane. The camera is equipped with a deep-depleted, back-illuminated CCD sensor (E2VDU934P) with a 13.3 mm $\times$ 13.3 mm active area, divided into 1024 $\times$ 1024 square pixels of 13 µm side. This setup delivers a pixel resolution of 1.68″ and a total field of view of 28.6′ $\times$ 28.6′. A 9-slot 28.5 mm filter-wheel positioned in front of the camera houses 6 interference filters composing the *ugrizy* photometric system, a Star Analyser 200

[†] https://www.nist.gov/laboratories/tools-instruments/primary-optical-watt-radiometer-powr-facility

diffraction grating, and a 0.2 mm pinhole, with one slot left vacant. The optical path includes the non-coated fused-silica window of the CCD cell, affected by a 0.5° wedge on the entry side. An axial degree of freedom allows to adjust the camera-filter wheel assembly over 9 cm range for precise focusing. The instrument, pictured in Figure 2, is fixed on a motorized equatorial mount. The instrument is fully robotic and allows for conducting remote observations.

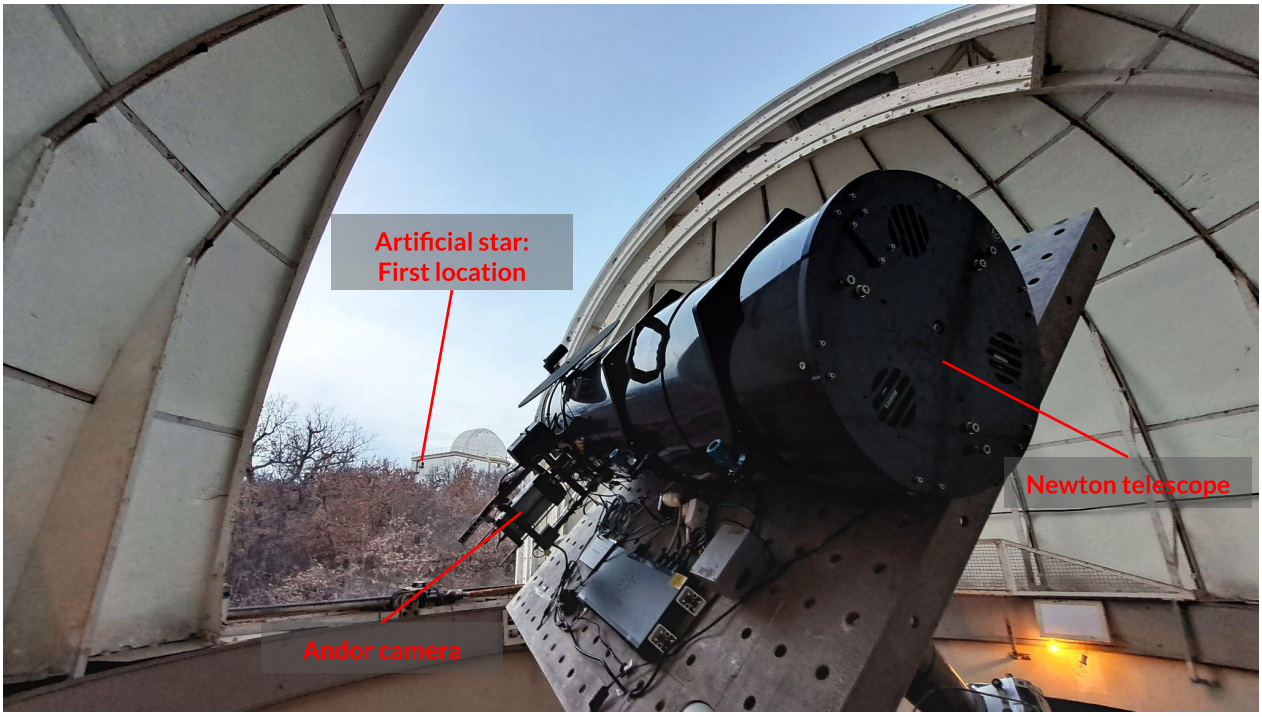

Figure 2. Photograph of the StarDICE telescope on its mount.

The instrument is hosted by l'Observatoire de Haute-Provence in the south of France, located at an altitude of ∼650 m above the sea level. The site has been chosen for the quality of its sky, which claims that for a 1 m diameter telescope, 30 ± 7 % of the nights are usable for relative photometry, and 10 % for absolute photometry[‡]. A satellite view of the site with the location of the StarDICE telescope and the artificial star is shown Figure 3.

2.2.1 Monitoring instruments

To monitor the environmental conditions of the observations, several monitoring instruments are installed, and taking data during the whole measurement campaign, are listed in the following:

- A WTX536 Vaisala weather station[§] combining a thermometer, a hygrometer and a barometer. It also provides a measurement of the speed and orientation of the wind with an ultrasound anemometer and a rain detector with a piezoelectric surface which detects the impact of the water drops. The main purpose of this instrument is to send a trigger signal if the meteorological conditions threaten to damage the setup, inducing an automatic closing of the dome slit to protect the telescope. In addition, the monitored temperature, pressure, and humidity are used to model the atmosphere and the atmospheric refraction.
- 3 thermometers and 1 hygrometer were installed on the telescope mount to control the environment inside the dome.
- An all-sky camera StarLightExpress Oculus to monitor the full sky visibility remotely.

[‡] http://www.obs-hp.fr/guide/stats_meteo.shtml
[§] https://www.fondriest.com/pdf/vaisala_wxt530_spec.pdf

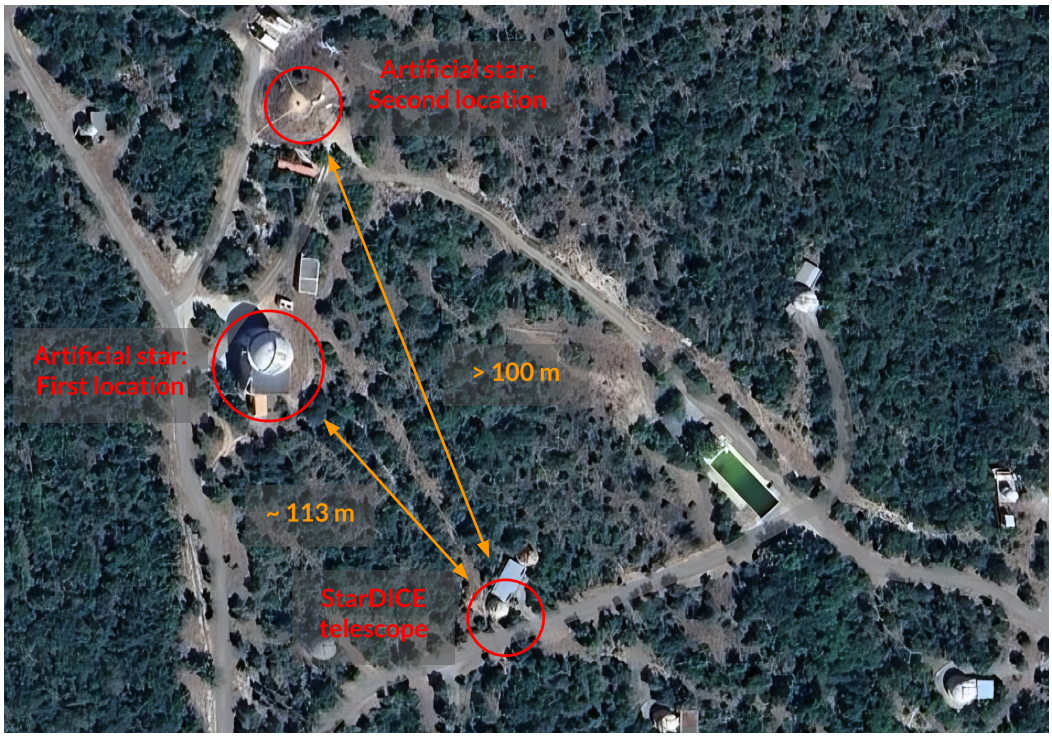

Figure 3. Satellite view of the StarDICE experiment location. The StarDICE telescope is mounted in the coupola at the bottom, while the artificial star is located in a building hosting another telescope (T152) for the pre-survey, at a distance of 113 m measured with laser telemetry, with an elevation of 8.3°. For the final stage of the survey, the star will be mounted on a pole located at the top of the picture, at a distance longer than 100 m, and an elevation higher than for the pre-survey location.

- Two webcams within the dome: one is fixed on the StarDICE tube, while the other is mounted on the wall. These cameras provide live feedback of the dome's interior to a remote observer.

2.3 StarDICE telescope throughput

The StarDICE telescope throughput and its filter transmissions will be monitored with the StarDICE artificial star during the whole survey. This source is shown in Figure 4, where we can see its 16 LEDs covering a wavelength range from soft-ultraviolet to near-infrared. An image of each LED is represented in Figure 5, obtained with a microscopic camera observing each light source individually. The calibration of this artificial star is ongoing and it will be mounted on site in the near future. For now, the telescope throughput measurement will rely on the work achieved in Souverin et al. 2022[4] and Souverin et al. in prep. 2024.

3. DATASET DESCRIPTION

3.1 StarDICE observations

The StarDICE instrument has been operating since early 2023, currently in a pre-survey phase dedicated to testing observing strategies. During this phase, it has accumulated approximately 30 nights of observations since September 2023. Prioritizing the observation of CALSPEC primary standards when they are observable, and secondary standards otherwise, several targets are observed throughout each night. The schedule is optimized to achieve the most complete airmass range between 1 and 2 for each source. For every target, observations are made successively with the filters g, r, i, z, y, u, and finally the diffraction grating, with 5 poses per band, repeating as necessary to cover the desired airmass range. Exposure times are optimized for each bandpass to achieve the best signal-to-noise (SNR) ratio without the CALSPEC star saturating the camera.

Figure 4. Picture of the 16 LEDs turned on which form the artificial star.

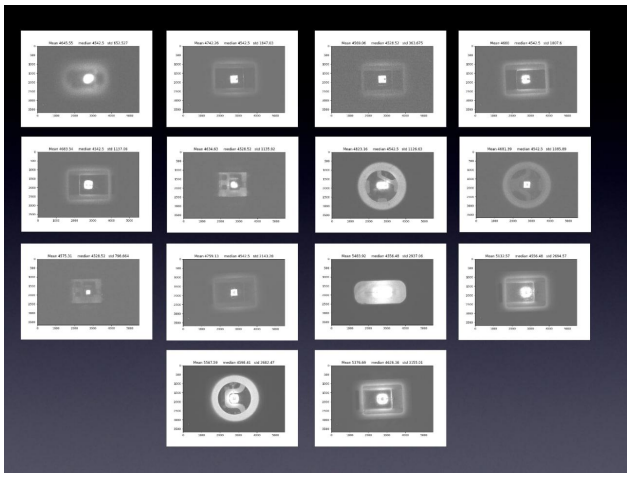

Figure 5. Laboratory observations of the artificial star LEDs, where a single LED is shown in every frame. For each LED, we can observe the surface brightness of its active core, and its enclosure which reflects emission light.

While several targets have been observed, special attention has been given to the CALSPEC primary standard G191B2B. The pointing of a specific target star is achieved with an accuracy of $1.5'$, with the target star at the center of the field. Each image thus yields the target star and a number $N_{\rm stars}$ of secondary field stars per exposure, of the order of between $\sim$400 and $\sim$650 for the *grizy* bands, and $\sim$76 for the u band. The total number of images, sources observed, and observation nights for the G191B2B dataset are compiled in Table 1. The number of visible sources is lower in the u band compared to others due to the low response of the StarDICE telescope at these wavelengths. This is illustrated in Figure 6, where we can see more sources in the r band than in the u band.

Table 1. Total number of images, sources, and night observations forming the StarDICE dataset for G191B2B.

	g	r	i	z	y	u	TOT.
$N_{\rm images}$	3251	3266	3385	3234	3369	3264	19769
$N_{\rm stars}$	413	654	424	398	450	76	792
$N_{\rm nights}$	23	23	23	23	23	23	23

3.2 Synthetic photometry

To recalibrate the standard star, we compare the observations to synthetic photometry where the photon flux F_{synth} reads:

$$F^{\rm synth} = \int_{\lambda} S_{\star}(\lambda) \times R_{\rm SD}(\lambda) \times T_{\rm atm}(\lambda, P_a) \times t_{\rm exp,SD} \times A_{\rm mirror,SD} \times \frac{\lambda d\lambda}{hc}, \quad (1)$$

with $S_{\star}(\lambda)$ the observed star SED; $R_{\rm SD}(\lambda)$ the response of the StarDICE telescope; $T_{\rm atm}(\lambda)$ the atmospheric transmission; $t_{\rm exp,SD}$ the exposure time; $A_{\rm mirror,SD}$ the collection surface of the StarDICE mirror; λ the wavelength; P_a a set of atmospheric parameters; and h and c respectively the Planck constant and the celerity of

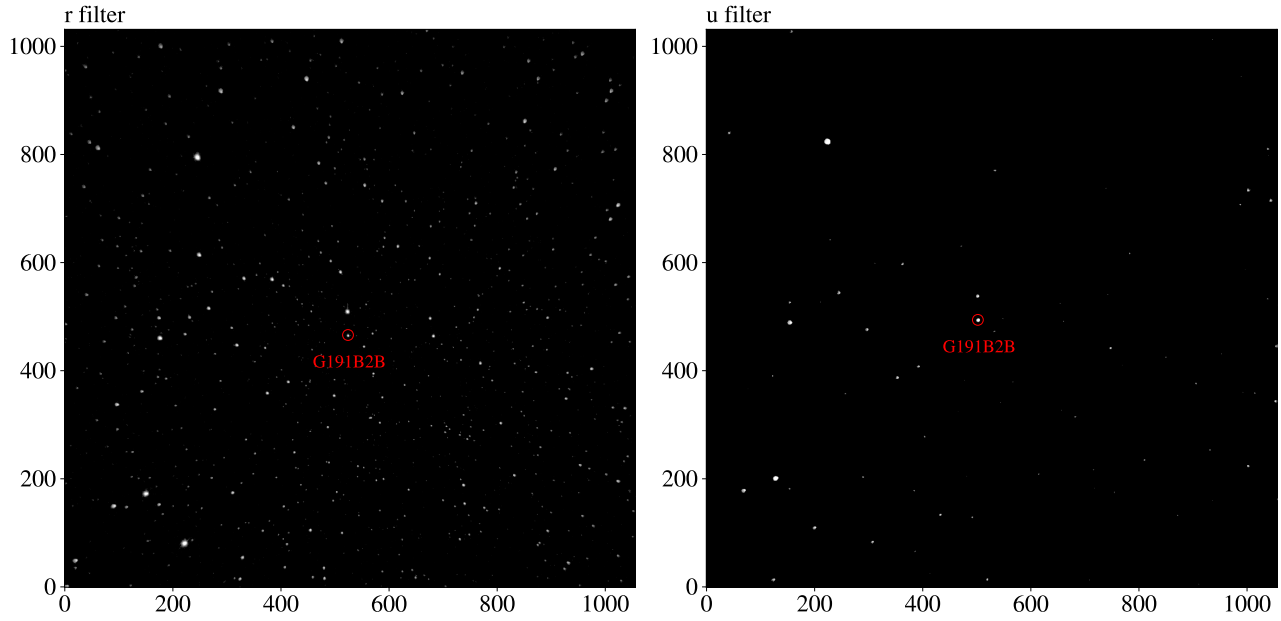

Figure 6. Two examples of images of the G191B2B field of view observed with the StarDICE instrument, with the r filter in the left, and the u filter in the right.

light. $t_{\mathrm{exp,SD}}$ and $A_{\mathrm{mirror,SD}}$ are known, and we have a prior measurement of $R_{\mathrm{SD}}(\lambda)$ from Souverin et al. 2022.[4] This response will be continuously monitored with the artificial star during the final survey.

The star SEDs are estimated with the low-resolution spectra provided by the Gaia DR3 (Montegriffo, Gaia collaboration et al. 2023[7], Gaia collaboration et al. 2016[8]). We use the GaiaXPy python library[¶] to fetch the spectra of stars in the G191B2B field of view.

The atmosphere transmission is simulated with the Libradtran software[‖] (Emde et al. 2016[9]). The set of parameters P_a used for atmospheric simulation includes three in-situ monitored parameters: airmass, temperature, and pressure. Pressure and temperature are measured at the ground level with the monitoring instruments presented in Section 2.2.1. The airmass can be inferred from the apparent altitude h at which the telescope is pointing, and with the formula from Pickering et al. 2002[10]:

$$X = \frac{1}{\sin(h + 244/(165 + 47h^{1.1}))}. \tag{2}$$

Additionally, three other parameters complete the P_a set: Precipitable Water Vapor (PWV, in mm), ozone quantity (in Dobson units), and Vertical Aerosol Optical Depth (VAOD). For this analysis, these parameters are fixed at values of 5 mm, 400 DU, and 0.1 respectively. This choice does not give an accurate representation of the atmosphere but allows for accounting for the variation in airmass in a night of observation, and pressure

[¶] https://gaia-dpci.github.io/GaiaXPy-website/

[‖] http://www.libradtran.org

from one night to another. In future analyses, these parameters will be fitted on the spectra observed with the diffraction grating, using the Spectractor software from Neveu et al. 2021[11].

Finally, synthetic photometry F^{synth} is computed for every source observed, for every exposition, and every filter.

4. DATA REDUCTION AND ANALYSIS

4.1 Aperture photometry

We want to measure the quantity of photons collected by the StarDICE camera from all astrophysical sources in the field of view. To achieve this measurement, we perform aperture photometry on each source. A necessary preliminary step is to subtract the overscan and background contribution to the image. The overscan of each image is estimated by averaging the rows of the vertical overscan, and the columns of the horizontal overscan, subtracting the corresponding estimation for each pixel. To estimate the background contribution, the sources in the image need to be detected and masked. We begin by computing the standard deviation σ of the image. Pixels with a signal higher than 5σ are masked, along with all surrounding pixels that have a signal higher than 2σ. The masked image is then segmented into boxes of 129×132 pixels. For each box, the mean and standard deviation of the background are calculated. These values are interpolated into a 2D map, providing an estimation of the background. This estimated background is subtracted from the image. Aperture photometry, consisting of the summation of all the pixels in a 5.6 pixels radius around the 5σ detected sources is performed, yielding the observed flux $F^{\mathrm{obs}}_{i,s}$ of each source s in exposure i.

4.2 Synthetic photometry vs. aperture photometry

4.2.1 Fitting method

In this section, we aim to quantify the discrepancy between synthetic and measured magnitudes for every image i taken at different airmasses X_i. The purpose is to extrapolate these quantities to zero airmass, which corresponds to the out-of-atmosphere difference between the synthetic and measured photometry. We must determine one value per filter, corresponding to the correction term we must apply to recalibrate the SED of the measured star.

To quantify the discrepancy between synthetic and measured magnitudes for a source s in an image i, we define $\Delta m_{i,s}$ as follows:

$$\Delta m_{i,s} = m^{\mathrm{obs}}_{i,s} - m^{\mathrm{synth}}_{i,s} = -2.5 \log_{10} \left(\frac{F^{\mathrm{obs}}_{i,s}}{F^{\mathrm{synth}}_{i,s}} \right), \tag{3}$$

with $F^{\mathrm{synth}}_{i,s}$ the synthetic flux described in Section 3.2, and $F^{\mathrm{obs}}_{i,s}$ the measured flux via aperture photometry. This variation can be decomposed as:

$$\Delta m_{i,s} = \Delta \mathrm{ZP}_i + \Delta m_s + \epsilon_{i,s}, \tag{4}$$

where $\Delta \mathrm{ZP}_i$ represents the mean difference of photometry for an image i, averaged over all sources s of the field of view; Δm_s represents the mean difference of photometry of a source s, averaged over all images i; and $\epsilon_{i,s}$ accounts for the random noise. This noise includes contributions from the background noise, and other contributions specific to the sensor such as readout, gain, and focal plane inhomogeneities noises. It follows a normal distribution $\mathcal{N}(0, \sigma_{i,s})$, and the standard deviation $\sigma_{i,s}$ can be modeled as a polynomial function of the inverse of the synthetic flux F^{synth}:

$$\sigma^2_{i,s} = \frac{A}{{F^{\star}_{i,s}}^2} + \frac{B}{F^{\star}_{i,s}} + C, \tag{5}$$

where A, B, and C account respectively for the readout and background noise; the photon noise; and the focal plane inhomogeneities, gain, scintillation, or aperture correction noise contribution. The model is fitted with an iterative method, computing at each iteration:

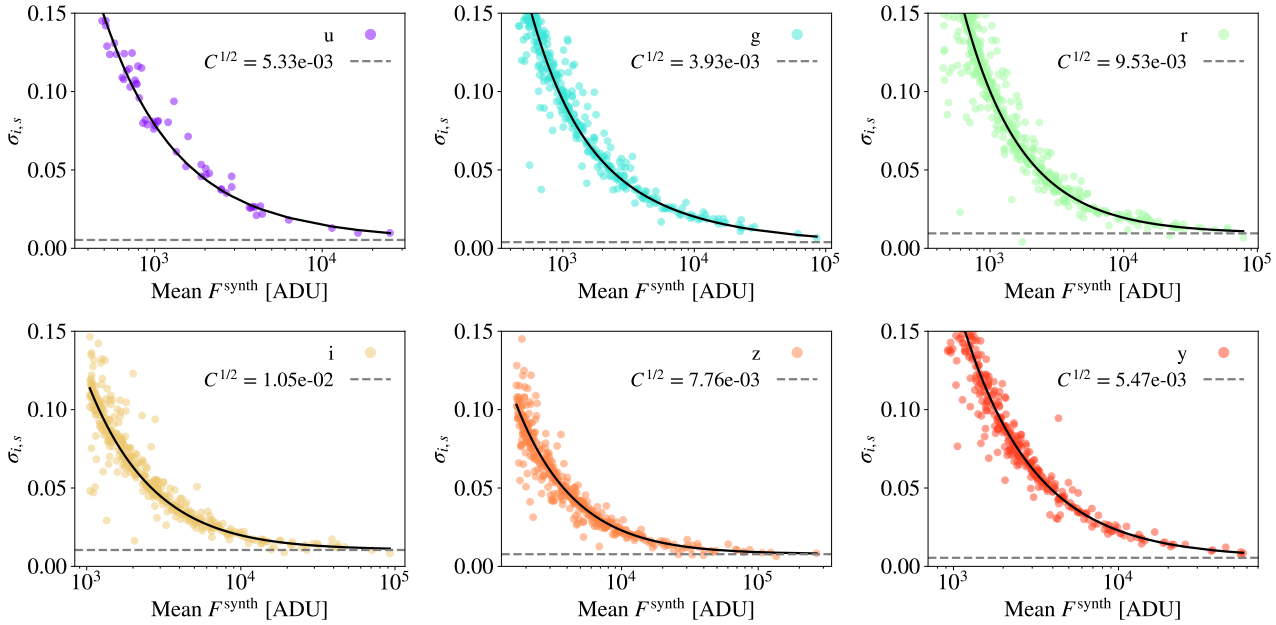

Figure 7. Standard deviation $\sigma_{i,s}$ of the normal distribution $\mathcal{N}(0, \sigma_{i,s})$ of the noise $\epsilon_{i,s}$ from Equation 3, against the mean synthetic flux F^{synth}. Each panel corresponds to a StarDICE filter. The model from Equation 5 fitted for each filter is represented by the plain dark line, while the dashed gray line represents the value of $C^{1/2}$, equivalent to the minimum dispersion when the flux tends to infinite positive values.

$$\Delta \mathrm{ZP}_i = \frac{\Sigma_s \dfrac{\Delta m_{i,s} - \Delta m_s}{\sigma_{i,s}^2}}{\Sigma_s \dfrac{1}{\sigma_{i,s}}} \quad ; \quad \Delta m_s = \frac{\Sigma_i \dfrac{\Delta m_{i,s} - \Delta \mathrm{ZP}_i}{\sigma_{i,s}^2}}{\Sigma_i \dfrac{1}{\sigma_{i,s}}}, \tag{6}$$

with $\sigma_{i,s}$ initially set to 1 and $\Delta m_s = 0$. The flux uncertainties $\sigma_{i,s}$ are estimated as the standard deviation of the residuals between the values of $\Delta m_{i,s}$ measured and fitted, which are represented in Figure 7. We fit the model from Equation 5 for each filter, updating the value of $\sigma_{i,s}$ for the next iteration of the fit. Outliers exceeding 5σ are rejected, and the process is repeated until no further outliers are identified.

To estimate the amount of flux missed when using an aperture of 5.6 pixels, we compare it to a larger aperture of 7.7 pixels. We define the quantity $C_i = \frac{F_i^{\mathrm{obs}}(5.6\mathrm{px})}{F_i^{\mathrm{obs}}(7.7\mathrm{px})}$, the mean aperture correction evaluated with the 20 brightest sources in an image i. Finally, we perform the following fit:

$$\Delta \mathrm{ZP}_i = k_i X_i + \alpha_i C_i + \mathrm{ZP}_0, \tag{7}$$

with ZP_0 is the estimation of the out-of-atmosphere discrepancy between the synthetic and the measured photometry. This provides a ZP_0 parameter for each filter, corresponding to the correction term to apply to the standard SED for recalibration. Figure 8 depicts $\Delta \mathrm{ZP}_i$ vs the airmass X_i for the 17$^{\mathrm{th}}$ of December 2023, and the residuals to the fit of Equation 7.

4.2.2 Rejection of non-photometric night

Figure 9 depicts the $\Delta \mathrm{ZP}_i$ residuals evolution for the 9$^{\mathrm{th}}$ of September 2023, where a noticeable extinction occurs in all bands between airmass ~ 1.4 and ~ 1.5. This is due to a cloudy period, causing a gray extinction, that is rejected as being detected and presenting a large variation with respect to the average atmospheric transmission of the night. Thus, we perform a rolling mean over all the filter residuals to detect any gray extinction, and outliers of more than 3σ are rejected, and the entire fit of $\Delta \mathrm{ZP}_i$ and Δm_s is performed again without these

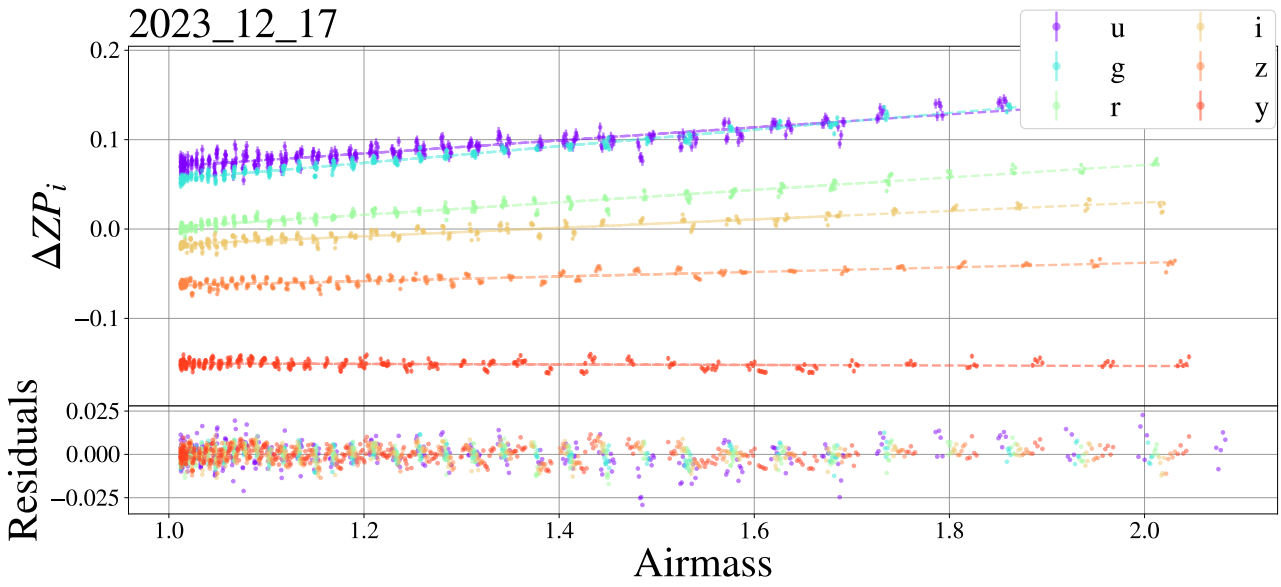

Figure 8. Top: ΔZP_i versus airmass for the G191B2B field of view observed the 17th of December 2023. Each color represents a StarDICE band. The dashed colored line represents the best linear fit for each band. Bottom: Residuals of the ΔZP_i subtracted by the best linear fit for each StarDICE band.

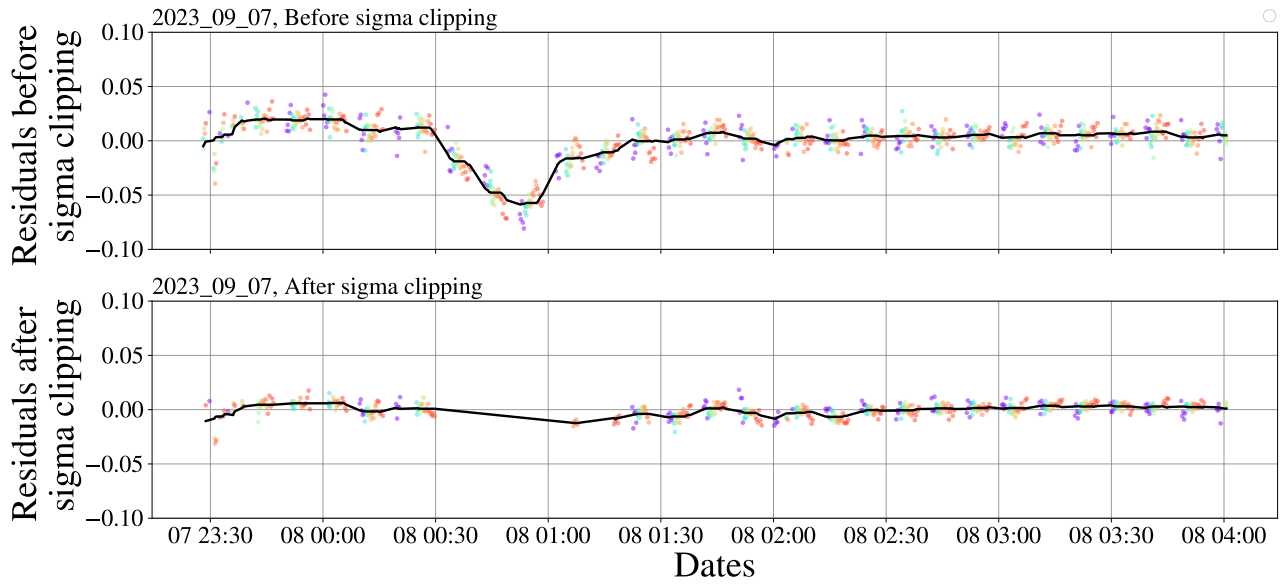

Figure 9. ΔZP_i residuals for the 9th of September 2023. The colored dots correspond to the different StarDICE bands as in Figure 8, while the plain black line corresponds to the rolling mean passing through all filters. The top panel shows residuals before the sigma clipping, while the bottom panel shows the residuals after the sigma clipping and a second iteration of the fit. All the bands see a significant drop between airmass ~ 1.4 and ~ 1.5, symptomatic of a gray cloudy period, that is detected and cut.

data points. Although this method allows for the rejection of an evident cloudy period, smaller gray extinctions persist and have not been detected yet. Figure 10 illustrates such an example of grey transmission variations visible in each band, but remaining below the 3σ level. To address this, an infrared camera will accompany the optical StarDICE telescope, measuring the sky's radiance to account for cloud extinction. More details about this instrument are provided in Section 5.2.1.

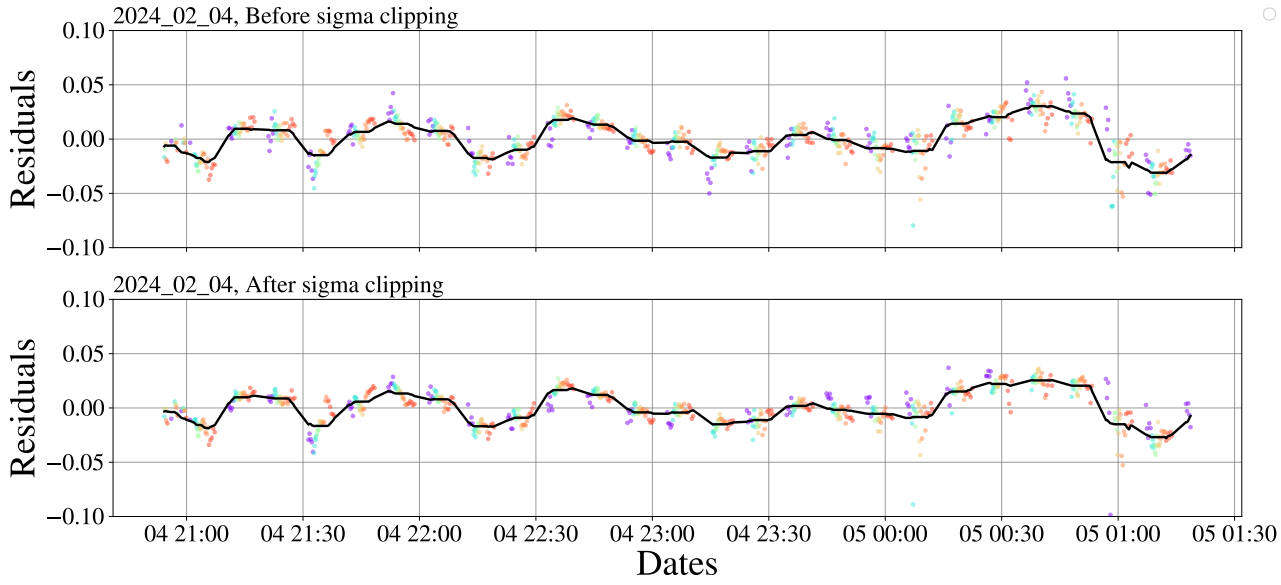

Figure 10. ΔZP_i residuals for the 4th of February 2024. The dots and lines represent the same as in Figure 9. For the entire duration of the observations, all bands are affected by small bumps, revealing poor photometric stability over the entire night. These bumps are not detected and the residuals are the same before and after the sigma clipping.

For now, to reject non-photometric nights that pass through the gray extinction rejection, we set a threshold for the standard deviation σ_{rolling} of the rolling mean during a night. If $\sigma_{\text{rolling}} > 5 \times 10^{-3}$, then we consider the night as non-photometric. Additionally, we reject nights with an airmass range of less than 0.3, and nights where the mean of the parameters k is higher than 0.1, a sign that the atmosphere model is not representative of reality. The residuals to the linear airmass regression per band and per night ranges between 3 mmag and 9 mmag.

4.3 Results

In this section, we present the results regarding the determination of this parameter and the predicted performance of the StarDICE experiment based on these findings. Figure 11 illustrates the dispersion of the ZP_0 parameter determined across the different nights and StarDICE bands. Since the ZP_0 represents the out-of-atmosphere difference between StarDICE measurements and synthetic photometry, it should remain constant for each filter. Our analysis aims to study the stability of ZP_0 values over different observations nights, to finally predict the number of nights needed for the StarDICE full survey to reach a 0.1 % level of accuracy. Figure 12 depicts the root mean square (RMS) of the ZP_0 parameter estimation in the top panel. The bottom panel shows the corresponding RMS divided by $\sqrt{N_{\text{nights}}}$ for a predicted observations night of $N_{\text{nights}} = 100$. This plot shows that in the current state of the analysis, StarDICE can provide a recalibration of the CALSPEC standard with an accuracy better than 0.4 % for the *griz* bands, and of approximately 0.6 % for the u and y bands.

The ZP_0 values fitted here cannot be used for recalibration because the instrument calibration is not monitored, which will be the case once the artificial star is mounted, as discussed in Section 5.2.3. Additionally, the instrument calibration from Souverin et al. 2022[4] and Souverin et al. 2024 in prep. indicate that the u and y band calibration cannot be trusted in the current situation. Only a portion of the u passband has been calibrated, while the y band calibration suffered from large aperture correction caused by an important degradation of the PSF of the instrument at these wavelengths.

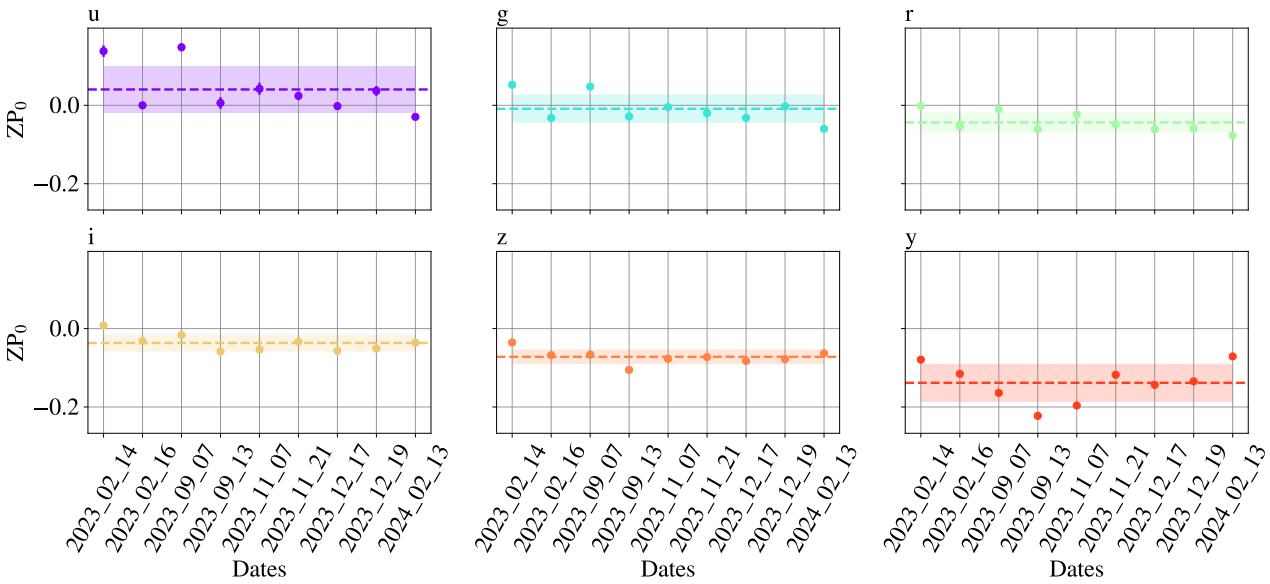

Figure 11. ZP_0 parameter fitted for the 9 photometric nights of observations, and every filter. The dashed lines represent the average estimation of ZP_0, while the transparent colored areas represent the standard deviation.

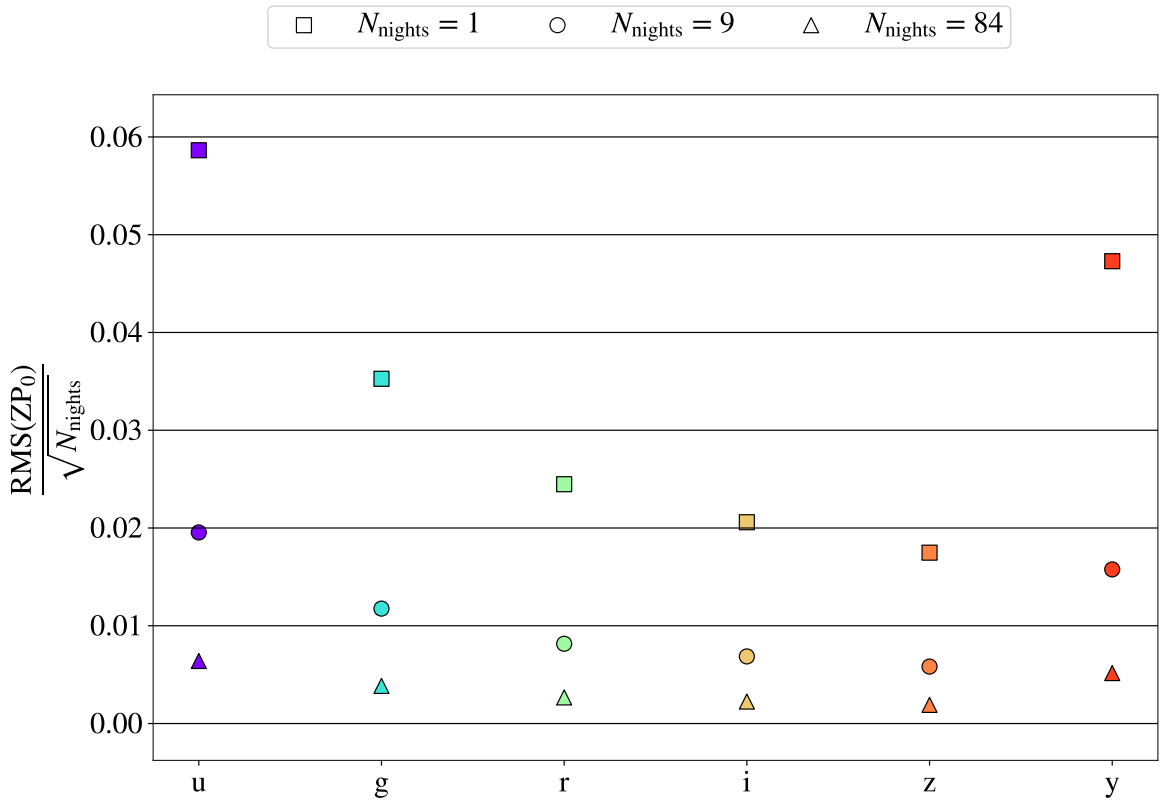

Figure 12. RMS of ZP_0 fitted for the 9 photometric nights of observations and for each StarDICE band, normalized by the square root of the number of nights. The square represents the RMS for one night of observations; the circles represent the RMS for the 9 photometric nights used in this analysis; the triangles represent the predicted RMS for 84 observation nights, corresponding to approximately 2 years of the StarDICE survey.

5. CONCLUSION AND FUTURE PERSPECTIVES

5.1 Summary

A pre-survey for the StarDICE experiment was conducted over a total of 23 nights, out of which 9 were deemed suitably photometric. In its current state of the analysis, StarDICE reconstructs top-of-the-atmosphere broadband magnitudes with a dispersion of 2 to 4 % per night for the z, i, r and g bands, for a selection of photometric nights representing ∼40 % of the observable nights. We can scale this performance to a 2-year survey, equivalent to ∼ 110 photometric nights from the numbers given by the observatory site in Section 2.2. Accounting for ∼40 % of nights kept, we end up with approximately 84 nights of observation and we estimate the top-of-the-atmosphere broadband magnitudes dispersion of 0.19 to 0.38 % for the z, i, r and g bands. This is approximately two to four times the suitable target needed to fully exploit LSST supernovæstatistics.

Interestingly, the observed dispersion in reconstructed top-of-the-atmosphere magnitudes for the selected photometric nights is still 5 to 10 times higher than the claimed statistical uncertainty inferred from the residual dispersion of the linear airmass regression for those nights. This indicates substantial deviations from the stable atmospheric transmission model that underpins the linear airmass regression, even during photometric nights. Ongoing work aims to improve the model and thereby enhance the performance of the calibration survey.

5.2 Future perspectives

5.2.1 Infrared camera

The presence of clouds in the sky is a challenge to achieve a sub-percent precision on the photometric measurement with StarDICE. Addressing this concern is among the conclusions drawn from the proof of concept outlined in the F. Hazenberg thesis[12]. To overcome this issue, we propose to use an uncooled infrared thermal camera (UIRTC) to evaluate astronomical observation quality concerning gray extinction contamination. The camera measures the radiance of the sky in the long-wave infrared range from 8 to 14 µm, where the contrast between a cloudy and a clear sky is relatively high (Shaw et al. 2005[13]). Hence, the purpose of this camera is at least to provide a flagging of the presence of clouds which induces non-photometric images, and at best to quantify the attenuation in the visible measurement of the StarDICE telescope. The camera is a FLIR Tau2[**], with a 640×512 vanadium oxide (VOx) pixels sensor coupled to a Umicore lens, providing a resolution of $1\,''$/pixel. This study is the subject of a work detailed in Sommer et al. in prep. 2024.

5.2.2 Fit of the atmosphere

Another major issue in this analysis is the accuracy of the atmosphere transmission model. Currently, the temperature and pressure parameters are monitored at the ground level, which is not representative of the environment in the line of sight. On the other hand, the PWV, VAOD, and ozone quantity are fixed. To perform a better atmosphere transmission model, we will use the data from the diffraction grating. Pursuing a slitless spectrophotometry analysis with the Spectractor software[††], we can fit the 6 above-mentioned atmospheric parameters. More details about the method are given in Neveu et al. 2021[11], where it is shown that the software can retrieve compatible atmospheric parameters with simulated data, and promising results with on-sky data, limited by systematic effects (view Section 5 of Neveu et al. 2021[11] for more details).

5.2.3 Artificial star

Lastly, part of the dispersion may originate from variations in the response of the photometric instrument itself. The next crucial step for StarDICE is the installation of the first artificial star, whose observations will be interleaved with those of the standard stars. These observations will enable both the monitoring of the photometric response stability and the absolute calibration of star magnitudes. The installation is planned for June 2024, followed by a short observation campaign to conclude the pre-survey.

[**] https://www.flir.fr/support/products/tau-2/?pn=Tau+2&vn=46336100H#Documents

[††] https://github.com/LSSTDESC/Spectractor

REFERENCES

[1] Bohlin, R. C., Hubeny, I., and Rauch, T., "New Grids of Pure-hydrogen White Dwarf NLTE Model Atmospheres and the HST/STIS Flux Calibration," *aj* **160**, 21 (July 2020).

[2] Bohlin, R. C., Gordon, K. D., and Tremblay, P. E., "Techniques and Review of Absolute Flux Calibration from the Ultraviolet to the Mid-Infrared," *pasp* **126**, 711 (Aug. 2014).

[3] Axelrod, T., Saha, A., Matheson, T., Olszewski, E. W., Bohlin, R. C., Calamida, A., Claver, J., Deustua, S., Holberg, J. B., Hubeny, I., Mackenty, J. W., Malanchev, K., Narayan, G., Points, S., Rest, A., Sabbi, E., and Stubbs, C. W., "All-sky Faint DA White Dwarf Spectrophotometric Standards for Astrophysical Observatories: The Complete Sample," *apj* **951**, 78 (July 2023).

[4] Souverin, T., Neveu, J., Betoule, M., Bongard, S., Brownsberger, S., Cohen-Tanugi, J., Dagoret-Campagne, S., Feinstein, F., Juramy, C., Le Guillou, L., van Suu, A. L., Blanc, P. E., Hazenberg, F., Nuss, E., Plez, B., Sepulveda, E., Sommer, K., Stubbs, C., Regnault, N., and Urbach, E., "Measurement of telescope transmission using a Collimated Beam Projector," in [*56th Rencontres de Moriond on Cosmology*], (Jan. 2022).

[5] Larason, T. C. and Houston, J. M., "Spectroradiometric detector measurements ::ultraviolet, visible, and near-infrared detectors for spectral power," (2008-01-01 05:01:00 2008). In: https://doi.org/10.6028/NIST.SP.250-41e2008.

[6] Betoule, M., Antier, S., Bertin, E., Blanc, P. É., Bongard, S., Cohen Tanugi, J., Dagoret-Campagne, S., Feinstein, F., Hardin, D., Juramy, C., Le Guillou, L., Le Van Suu, A., Moniez, M., Neveu, J., Nuss, É., Plez, B., Regnault, N., Sepulveda, E., Sommer, K., Souverin, T., and Wang, X. F., "StarDICE. I. Sensor calibration bench and absolute photometric calibration of a Sony IMX411 sensor," *aap* **670**, A119 (Feb. 2023).

[7] Gaia Collaboration, Vallenari, A., Brown, A. G. A., Prusti, T., J., d. J. H., et al., "Gaia Data Release 3. Summary of the content and survey properties," *aap* **674**, A1 (June 2023).

[8] Gaia Collaboration, Prusti, T., de Bruijne, J. H. J., Brown, A. G. A., Vallenari, A., et al., "The Gaia mission," *aap* **595**, A1 (Nov. 2016).

[9] Emde, C., Buras-Schnell, R., Kylling, A., Mayer, B., Gasteiger, J., Hamann, U., Kylling, J., Richter, B., Pause, C., Dowling, T., and Bugliaro, L., "The libRadtran software package for radiative transfer calculations (Version 2.0)," *Geoscientific Model Development Discussions* **8**, 10237–10303 (Dec. 2015).

[10] Pickering, K. A., "The Southern Limits of the Ancient Star Catalog and the Commentary of Hipparchos," *DIO* **12**, 3–27 (Sept. 2002).

[11] Neveu, J., Brémaud, V., Dagoret-Campagne, S., and Fisher-Levine Merlin, "Spectractor: Spectrum extraction tool for slitless spectrophotometry." Astrophysics Source Code Library, record ascl:2104.004 (Apr. 2021).

[12] Hazenberg, F., *Calibration photométrique des supernovae de type Ia pour la caractérisation de l'énergie noire avec l'expérience StarDICE*, theses, Sorbonne Université (Sept. 2019). https://theses.hal.science/tel-02950846.

[13] Shaw, J., Nugent, P., Pust, N., Thurairajah, B., and Mizutani, K., "Radiometric cloud imaging with an uncooled microbolometer thermal infrared camera," *Optics express* **13**, 5807–17 (08 2005).